Photo-patternable hybrid ionogels for electrochromic applications

Andrew Kavanagh[a], Robert Copperwhite[b], Mohamed Oubaha[b], Jessica Owens[a], Colette McDonagh[b,c], Dermot Diamond[a] and Robert Byrne*[a].

[a] *CLARITY, The Centre for Sensor Web Technologies, National Centre for Sensor Research, School of Chemical Sciences, Dublin City University, Glasnevin, Dublin 9, Ireland. Tel: (00353) 17006009.*

[b] *Optical Sensors Laboratory, National Centre for Sensor Research, Dublin City University, Glasnevin, Dublin 9, Ireland.*

[c] *Biomedical Diagnostics Institute (BDI), Dublin City University, Dublin 9, Ireland.*

E-mail: Robert.byrne@dcu.ie

Abstract:

This work describes the development of photopatternable ionogels based on a hybrid organic/inorganic sol-gel material and both phosphonium (Trihexyltetradecyl-phosphonium dicyanamide [$P_{6,6,6,14}$][dca], trihexyltetradecylphosphonium bis(trifluoromethanesulfonyl)-amide [$P_{6,6,6,14}$][NTf2]) and imidazolium (1-ethyl-3-methylimidazolium tris*(pentafluoroethyl)trifluorophosphate [emIm][FAP]) room temperature ionic liquids (RTIL's). Ionogels were prepared via a two step process with RTIL content varied between 40-80 w/w%, and characterised via Raman and Electrochemical Impedance Spectroscopy. 1 and 2 photon polymerisation was performed on the hybrid ionogels using photolithography, resulting in three dimensional structures that were characterised using scanning electron microscopy. Electrochomic ionogels were prepared by addition of ethyl viologen dibromide (EV) to an ionogel containing [emIm][FAP] and hybrid sol-gel material. This composition was photo-polymerised on ITO electrodes by UV irradiation and subsequentially characterised via UV/Vis spectroelectrochemistry. It was also possible to fabricate a solid state electrochromic device based on EV and switch between the colourless (oxidised) and blue (reduced) forms using a perturbation signal of 1V.*

Introduction:

Room Temperature Ionic liquids (RTIL's) can be described as organic salts that are liquid at room temperature[1, 2]. Of their many favourable physicochemical properties -including negligible vapour pressure and tunable viscosity, density, melting and boiling points [3-5]- their intrinsic ionic conductivity and wide electrochemical window have attracted much research interest over the last decade as alternative electrolytes[6, 7]. For most engineering applications however, a solid electrolyte medium is preferable as leakage issues can complicate device fabrication.

Ionogels are a new type of hybrid materials which consist of an IL confined within a gel-like material[8, 9]. There are two possible routes for the incorporation of IL's in the gel, the organic route (polymer) which involves *in situ* polymerization or swelling of polymers with ILs[10]; and the inorganic route involving sol-gel methods or impregnation of ILs with oxide particles[11]. A particularly good review concerning the organic route is covered by Ueki and Watanabe.[12] This work is more concerned with the latter, i.e. the oxide route to encapsulation of ILs within a solid medium. Vioux *et al* have pioneered the process of confining ILs within an oxide matrix through a one step process.[13]

Ionogels offer many advantageous properties, including ionic conductivities similar to that of the pristine IL, transparency, mechanical robustness, flexibility, and the ability to engineer and mould into various dimensions, thus making them promising components in new solid-state electrolytes[14].

There have been few reports of ionogel applications in catalysis and luminescent devices[15]. We believe that ionogels could form the basis material for next generation opto-electronic devices due to the unique mechanical and electrochemical properties endowed on the ionogel by the IL, but if ionogels are to be used in the optoelectronics industry, more cost effective and efficient methods of fabrication will be needed to replace the pot-synthesis method.

Herein, we describe the synthesis and characterisation of phosphonium and imidazolium based ionogels and show 2- and 3D photo-patterned ionogel structures with nano resolution. The fabrication of an electrochromic ionogel device containing the electrochromic dye *ethyl viologen dibromide* is also described.

Experimental:

Chemicals and Materials:

Trihexyltetradecyl-phosphonium dicyanamide [$P_{6,6,6,14}$][dca] and trihexyltetradecylphosphonium bis(trifluoromethanesulfonyl)-amide [$P_{6,6,6,14}$][NTf2] were obtained compliments of Cytec® Industries.
Further purification was achieved by washing with both water and hexane, and by column chromatography. IL's were then dried under vacuum at 40 ^{o}C for 48 h, and stored under argon at 20 ^{o}C.[16]

1-ethyl-3-methylimidazolium *tris*(pentafluoroethyl)trifluorophosphate [emIm][FAP] was obtained compliments of Merck® industries.

Indium Tin Oxide (ITO) coated polyethylene, Poly(3-octylthiophene-2,5-diyl)(POT),
3-methacryloxypropyltrimethoxysilane(MAPTMS, Assay ~99% in methanol), zirconium (IV) n-propoxide (ZPO), Assay ~70% in propanol) and methacrylic acid (MAAH, $C_4H_6O_2$, Assay ~98%), 2,2-Dimethoxy-2-phenylacetophenone (DMPA) and Ethylviologen dibromide (EV) were used as purchased from Sigma-Aldrich® Ireland.

Hybrid Sol-gel Synthesis:

The sol-gel synthesis was based on the formation of a stable and homogeneous material obtained from the reaction between photosensitive organically modified precursors MAPTMS,ZPO and MAA; these were allowed to react in a molar ratio of 10:4:4; generating the hybrid material SZ4.

MAPTMS was first pre-hydrolysed with an aqueous solution (HCl 0.005 M), employing a 1.00 : 0.75 water to alkoxide molar ratio. As MAPTMS and water are not miscible, the hydrolysis was performed in a heterogeneous way. After 20 min of stirring, the production of methanol became sufficient to allow the miscibility of all species leading to a transparent solution. In parallel, to control the hydrolysis–condensation of ZPO and avoid the formation of any undesired ZrO_2 precipitate. MAAH was used as a chelating agent as it covalently binds with the zirconium atom through two oxygen atoms. The role of the chelating agent is directly related to the thickness of the resultant photopatterned waveguide; as descibed in a previous report[17].

This was done by employing a stoichiometric molar ratio of MAAH to ZPO. After 45 minutes of reaction, the pre-hydrolysed MAPTMS solution was added dropwise to the zirconium complex, characterised by an exothermic reaction.

Following another 45 minutes of reaction, in order to improve the homogeneity of both molecular systems, a second hydrolysis employing water (pH 7) was performed leading to a hydrolysis of 50 % of the total alkoxide groups. The final sol was left stirring for 24 hours before use.

Ionogel Synthesis

e.g. SZ4: [P_{66614}][dca] 60:40 w/w

600mg of SZ4 was mixed thoroughly with 400mg of [P_{66614}][dca] and 5wt% of photoinitiator (DMPA). The ionogel solution was sonicated for 5 minutes to ensure the photoinitiator was dissolved fully. It was then transferred to a 2cm diameter circular mould and photopolymerized with a UV BondWand (Electro-lite ®, Connecticut 20W,365 nm) for 10 minutes. The ionogel was placed in a vacuum oven at 50^0C for 24 hours. All ionogel combinations, as described in table 1 were prepared in accordance to the above procedure, with adjustments only to the hybrid organic sol-gel and IL proportions.

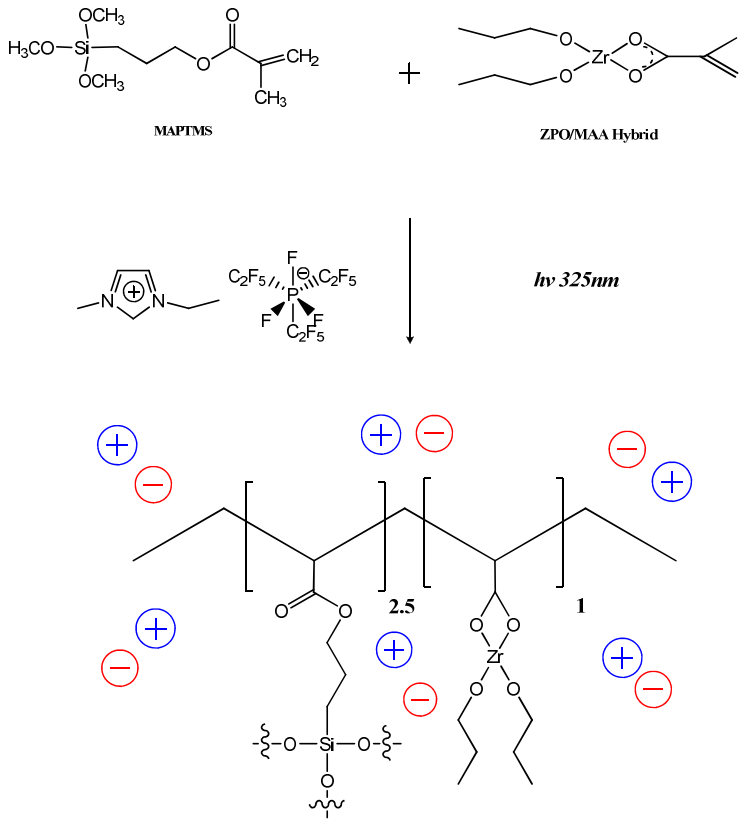

Scheme 1: Synthesis and possible structure of Hybrid, Photopatternable Ionogels.

Photo-patterning of Ionogels:

Photopatterning of the material was done on thin films which were formed by spin-coating. In this study, prior to deposition the sol was filtered through a 0.2 μm filter and then spin-coated onto a silicon wafer which had already been coated with a standard photocurable sol-gel material (no ionic liquid) which acted as a stable buffer layer. Spin-coating was carried out in a saturated alcohol atmosphere, as this helps to stabilize the evaporation rates of the solvents from the ionogel during coating, thus improving the quality of the thin film.

To achieve the desired coating thickness of 6-7 μm from the ionogel containing 20% IL, a rotation speed of 1500 rpm was employed. Fabrication of the photopatterned structures was carried out by UV exposure using the direct laser writing process. The laser writing system comprises a He–Cd laser (Kimmon Electric Co. Ltd, λ = 325 nm) and a computer-controlled two-axis linear motor system.

The co-ordinated movement of both axes of the linear motors moves the ionogel thin film beneath the stationary laser beam polymerizing the film as it moves. This permits the direct imprinting of any desired pattern in the ionogel.

The speed of movement of the ionogel coating beneath the laser beam was maintained at a constant 0.6 mm/s throughout all experiments. In order to evaluate the photoreactivity of the ionogel (20% IL), simple photopatterned lines were written over a range of UV energy densities (from 100–2200 $mJ.cm^{-2}$).

The laser beam energy was controlled by a computer-controlled acousto-optical modulator, which is synchronized with the linear motors through a custom-written Visual Basic user interface. After UV laser writing, the samples were rinsed in 1-butanol for 20 s in order to etch unexposed regions of the coatings, thus revealing the photopatterned ionogel microstructures.

Two-photon polymerization is a direct laser writing technique, which allows the fabrication of complex 3D structures with a resolution below 100 nm. In the present work, a Ti:sapphire laser was used (Chameleon, Coherent), delivering pulses of 140 fs duration at a repetition rate of 80 MHz with a central emission wavelength of 780 nm. A 100X microscope objective lens (Zeiss, Plan Apochromat, N.A. = 1.4) was used to focus the laser beam into the volume of the photosensitive material. The complete experimental setup and procedure has been described elsewhere[18].

Electrochromic Device Fabrication:

The first step in the device fabrication was to photopolymerise (for 10mins) the electrochromic ionogel into a pattern directly onto ITO using a specialised UV chrome photomask.

Once polymerised the resultant patterns were etched with ethanol and allowed to dry for a further 10 mins (fig 6 (left)).

The original ionogel material (without dye) was then applied around the electro-active patterns to facilitate the prospective current being passed through the device.

Finally an electrical seal was then generated by placing the top ITO layer atop of the liquid ionogel, and photo-polymerising through the ITO for a further 10 mins.

Instrumentation:

Electrochemical Impedance Spectroscopy was performed using the CHI® Instruments 660A potentiostat.

The frequency range scanned ranged from 1 MHz to 0.01 Hz, and the perturbation signal applied was 100mV. A platinum and Ag/AgCl were used as the reference and counter electrodes respectively and a nF capacitance shunt bridge was used in order to reduce high frequency noise.

In house, screen- printed, carbon paste silver electrodes were used as the working electrode, as described in a previous report[19]. The working electrodes were initially covered in a layer of POT (10^{-2}M in chloroform) and allowed to dry in order to aid the transfer of ionic to electronic conduction. 40μL of the ionogel to be analysed was then drop-cast and photo-polymerised @365nm for 10 minutes onto the POT layer.

Ionogel thickness was estimated using a Mitutoyo® vernier calipers calibrated to a resolution of 1μm.

Raman Spectroscopy was performed using the Perkin Elmer® Raman Station 400F.

Spectroelectrochemistry was performed by using a Cary 50 Probe® UV/Visible spectrophotometer and a CHI® Instruments 660A potentiostat in tandem.

Results and Discussion:

Raman spectroscopy:

The hybrid material SZ 4 (excluding ionic liquid) was initially characterised by raman spectroscopy, see figure S1 (a)-(c). The strongest Raman signals are located in the CH stretching region (2800–3000 cm^{-1}), assigned to the CH stretching vibrations of the MAPTMS alkyl chains. Several other distinct vibrational bands are present in the SZ material. The bands located at 1716 and 1640 cm^{-1} correspond to the ν(C = O) vibrations in MAPTMS and MAA, respectively.

In addition, the COO- rocking and deformation modes are apparent as a single vibration at 656 cm^{-1}. This bands confirm the chelation of the zirconium by the caroboxylate groups in MAA, as described previously.[20] The ν(C - O) band at 942 and 976 cm^{-1}, can be assigned to the bending mode of a bridging carboxylate group in a bidentate configuration of zirconium.

SiO_2 network vibrations are observed at 382 cm^{-1}; whilst the zirconium content in SZ4 can clearly be seen in the regions of 400- 950 cm^{-1} due to the emergence of bands at 418, 510, 656, 700 and 942 cm^{-1}.

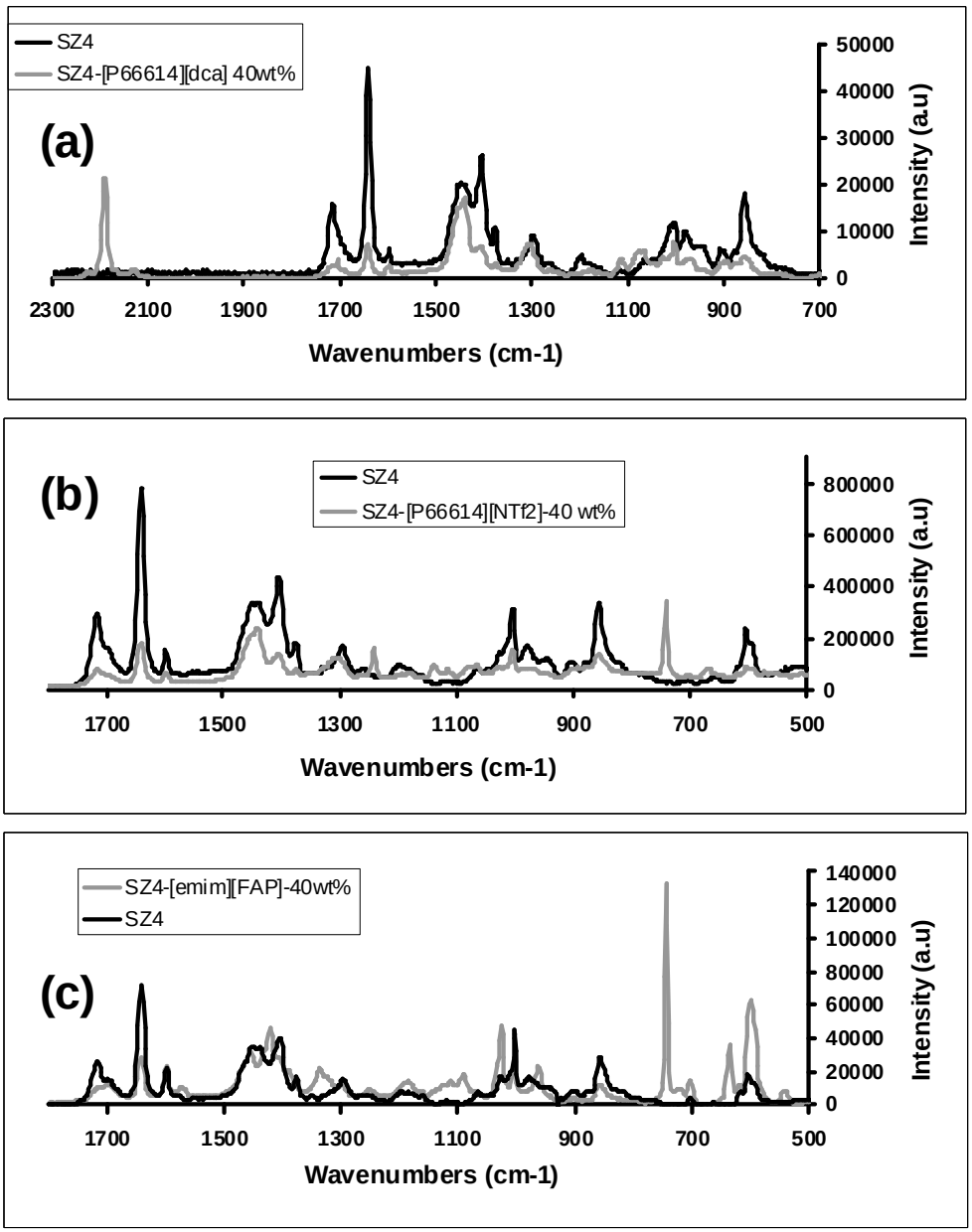

Fig. 1: Raman spectroscopy for (a) $[P_{6,6,6,14}][DCA]$, (b) $[P_{6,6,6,14}][NTf_2]$ and (c) [emIm][fap] in SZ4 hybrid ionogel.

In order to confirm the encapsulation of the IL's used within the hybrid material; ionogels containing 40wt% IL were next characterised. Figure 1 (a) above shows the Raman spectrum of the SZ4 hybrid material, and the SZ4-[$P_{6,6,6,14}$][dca] 40 wt% ionogel.

This spectrum clearly shows the incorporation of [$P_{6,6,6,14}$][dca] within the ionogel structure; as the signature nitrile (-C≅N) stretch from the $[dca]^-$ anion in the IL can be seen at 2188 cm^{-1}.

This is similar to the reported nitrile stretch in pristine [$P_{6,6,6,14}$][dca][21]. Equally the signature (–C=O) signature vibrations of the SZ4 material (as previously discussed) can also be seen at 1716 and 1640cm^{-1}.

Similarly, figure 2 (b) represents the SZ4-[$P_{6,6,6,14}$][NTf_2]-40 % ionogel. Assignable vibrations from the [NTf_2] anion are the SO_2 symmetric stretching (1136 cm^{-1}), and a SO_2 antisymmetric stretch with contributions from the CF_3 symmetric stretching mode (1242 cm^{-1}). In addition, the signature CF_3 symmetric bending band is located at 740 cm^{-1}. No significant vibrational deviations for [$P_{6,6,6,14}$][NTf_2] were observed when immobilised within the SZ4 matrix.

Figure 2 (c) presents the Raman spectrum obtained for SZ4-[emIm][FAP]-40 wt% ionogel. This spectrum also shows the incorporation of the imidazolium IL into the SZ4 ionogel, indicated by the presence of the signature C-F stretching at 744 cm^{-1}.

The characteristic C=N contributions of the imidazolium cation to the spectrum are located at both 1596cm^{-1} and 744cm^{-1}. Similar to the phosphonium based ionogels, [emIm][FAP] vibrational bands were not strongly influenced by the hybrid silicato-zirconate material ionogel matrix.

Electrochemical Impedance Spectroscopy:

EIS was first used to determine the effects of increasing the concentration of all 3 IL's on the SZ4 ionogel. This is best analysed via the "Bode" plot (Figure S2 (a) and (b)) which depicts the relationship between the modulus of impedance (Z) of the sample and the frequency scanned.

As the concentration of the IL in the SZ4 matrix increased, the expected complementary decrease in impedance was observed across the whole frequency range for all IL concentrations. The IL/SZ4 composites also display stable ionic conductivity, given that a linear increase in impedance is seen at both the high (electronic) and low (proton) frequency extremes.

The impedance of a system is also routinely expressed as a complex number. The resulting "Nyquist" plot is used to depict the relationship between real (Z') and imaginary (-Z'') components of impedance, of which the x-axis intercept is used to quantify the resistance of charge transfer (R_{CT}) of the system.

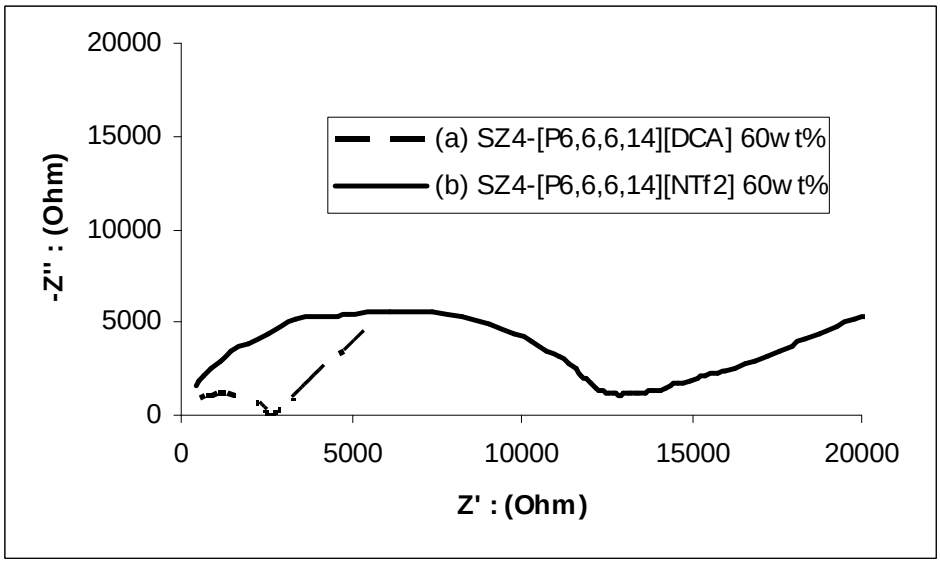

Fig. 2: Nyquist plots obtained for (a) 60wt% $[P_{6,6,6,14}][DCA]$ and (b) 60wt% $[P_{6,6,6,14}][NTf_2]$ in SZ4 gel.

Ionogel Composition:	***R_{CT}:***	σ: (S/cm^2) :
$[P_{6,6,6,14}]$[dca] : SZ4 (wt%. IL)		
40	12100	7.2×10^{-6}
60	2680	3.25×10^{-5}
$[P_{6,6,6,14}][NTf_2]$: SZ4 (wt%. IL)		
40	85420	1.02×10^{-6}
60	12980	6.72×10^{-6}
[emIm][fap] : SZ4 (wt.% IL)		
50	565	1.54×10^{-4}
80	278	3.14×10^{-4}

Table 1 : Ionogel composition, R_{CT} and conductivity values obtained from EIS for IL's in SZ4 gel.

R_{CT} is then easily converted to conductivity via the equations G = 1/R, and σ =GL / A.; where G is the conductance, R is the resistance, σ is the conductivity, L is the ionogel thickness between the two electrodes and A is the cross sectional area of the ionogel[22, 23]. Our in-house electrodes have a sensing surface area of $9mm^2$,[19] the ionogel thicknesses for each %wt. IL content is shown in fig S3 (a-d). For this the average thickness across 7 ionogels dropcast with the same initial volume were calculated and used as *L*.

The R_{CT} values were obtained from the resulting Nyquist plots (figure S4) for both phosphonium based IL's at both concentrations in the SZ4 gel and are summarised above in table 1. Both parameters were used to estimate the resulting conductivity of the ionogel on the working electrode.

The clear difference in conductivity as a function of the phosphonium IL anion can be seen from both table 1 and figure 2. It was found that ionogels containing the $[DCA]^-$ anion were of higher conductivity than their $[NTf_2]^-$ counterparts, which is in agreement with previous studies on the neat ionic liquid;[4]

and is most likely due to extensive electron delocalisation present in the $[DCA]^-$ ion and it being a comparably smaller ion than $[NTf_2]^-$.

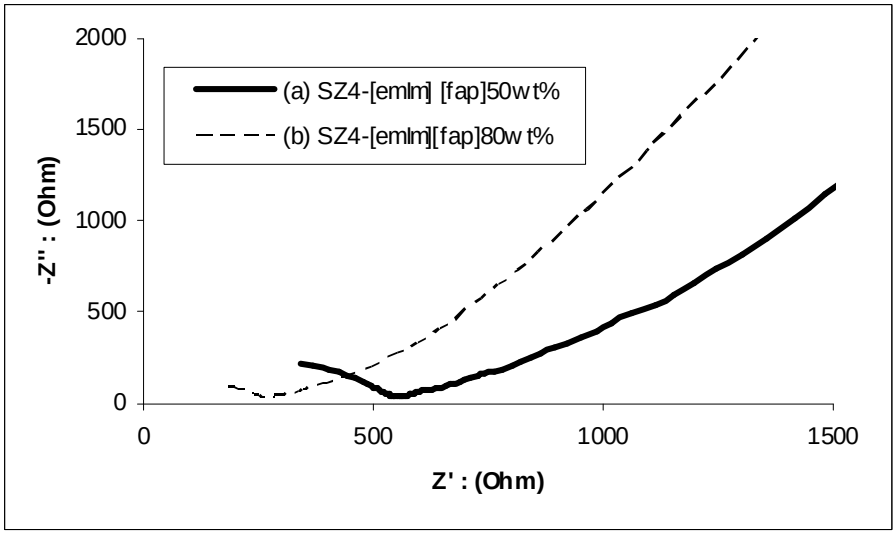

Fig. 3: Nyquist plots obtained for (a) 50wt% [emIm][fap] and (b) 80wt% [emIm][fap] in SZ4 gel.

In order to improve the conductivity of the ionogels further, the low viscosity IL [emIm] [FAP] was added at 50 and 80 wt% concentrations and analysed by EIS.
The resultant Nyquist plots can be seen above in figure 3, the converted conductivity values are again listed in table 1.

The conductivity of both films dramaticallly increased when compared to previous results, which is most likely due to mainly the comparibly low viscosity (75cP @ 25^0C) of the [emIm][FAP] IL but also possibly due to increased charge distribution.

The cationic charge of imidazolium based IL's are largely delocalized due to the extensive π-bonding of the heterocycle. Compare this to the phosphonium based IL's whose cationic charge are largely alkyl-shielded; and the vast change in conductivity is accounted for.

Planar and 3-D photopatterned structures:

The hybrid material SZ4 contains both Si and Zr acrylate modified alkoxides; which permits polymerisation via UV light irradiation. Both inorganic and organic parts form the basis of a co-hybrid material, which co-exist in a sub-micron biphasic system. The contribution of both of these phases results in this material whose properties have been extensively studied previously as photo-patternable channel waveguides with a low refractive index for use in optoelectronic communications[24, 25].

Experiments to demonstrate the photopatternability of the RTIL based novel materials were carried out using SZ4 containing 20% [$P_{6,6,6,14}$] [DCA] in conjunction with a direct laser writing process. The microstructures shown in Figure 3.1(c) and (d), show both a cross-sectional and top-down view of the photopatterned ionogel thin films. It can be seen from Figure 3(c) that as the UV exposure dose is decreased from left (5 x 3 μm) to right (4 x 1.5 μm) that the size of the resulting microstructures also decreases.

This demonstrates that the dimensions of these microstructures are sensitive to the UV exposure dose as is the case for standard photocurable hybrid sol-gel materials. These results clearly demonstrate the potential of these conductive materials to be exploited in high resolution photopatterning processes.

A woodpile structure fabricated employing the 2PP technique is presented in figure 4. In comparison with commonly used liquid resins in 2PP processing, this material allows the fabrication of PCs exhibiting negligible shrinkage, which avoids any further mechanical compensation.

This is essentially attributable to the particular molecular structure of the hybrid ionogel, in which both organic and inorganic moieties can form interconnected networks leading to high molecular cohesion.

First, the hydrolysis and condensation reactions taking place during the sol-gel synthesis allow the formation of polycondensable M-OH (M = Si, Zr) groups capable of forming strong and irreversible covalent bonds (Si-O-Si, Zr-O-Zr, and possibly Si-O-Zr).

Upon 2PP irradiation, the pendant methacrylate groups contained in the MAPTMS are crosslinked, resulting in the formation of irreversible and fully saturated aliphatic C-C covalent bonds, which penetrate throughout the irradiated region of the film.It is thought, in agreement with a recently reported study[26], that this

has the effect of confining the other constituents of the sol (zirconate complex and IL).

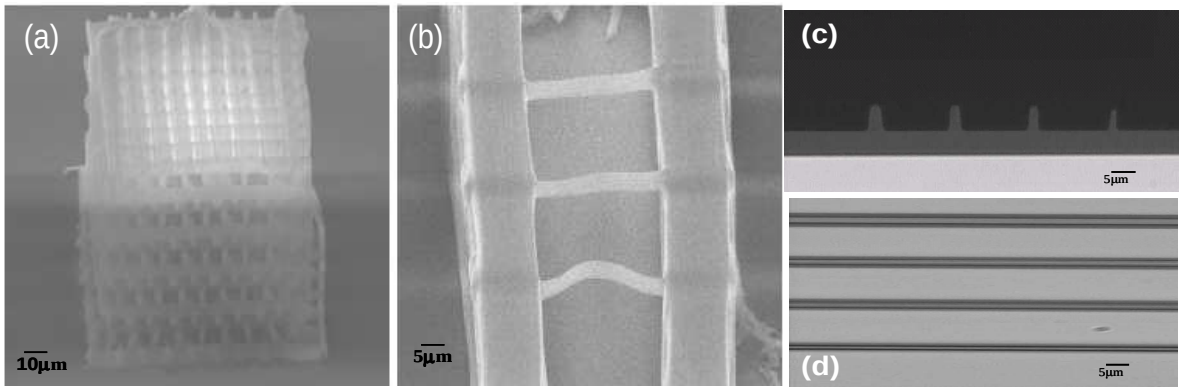

Fig. 4: (a) and (b) SEM images of three-dimensional woodpile structures from SZ4-20wt% [$P_{6,6,6,14}$][DCA] (c) and (d) Photopatterning of SZ4-20wt% [$P_{6,6,6,14}$][DCA].

Viologen spectroelectrochemistry and device fabrication:

The *Viologens* (or 1,1'-disubtituted-4,4'-bipyridines) are a class of electrochromic materials that have been shown to exist in three distinct redox states (Scheme 2)[27, 28].

Of the three, the dicationic salt (EV^{2+}) is the most stable and is colourless. Reductive electron transfer of the dicationic salt results in the formation of a highly coloured radical cation ($EV^{\cdot+}$), this process is completely reversible via re-oxidation of the $EV^{\cdot+}$ moiety. Somewhat less irreversible however, is the complete reduction of the radical cation to the colourless quinoid based EV^0. Irreversibility has been attributed to the latter's insolubility in polar electrolyte solvents[27].

In keeping with previous EIS data, an ionogel containing 50wt% [emIm][fap] and SZ4 was prepared using DMPA as the photoinitiator. The concentration of the viologen dye was 5 x 10^{-2} M within the ionogel. [emIm][FAP] was chosen for its increased ionic conductivity over its phosphonium based analogues in order to improve the kinetics of $EV^{\cdot+}$ formation.

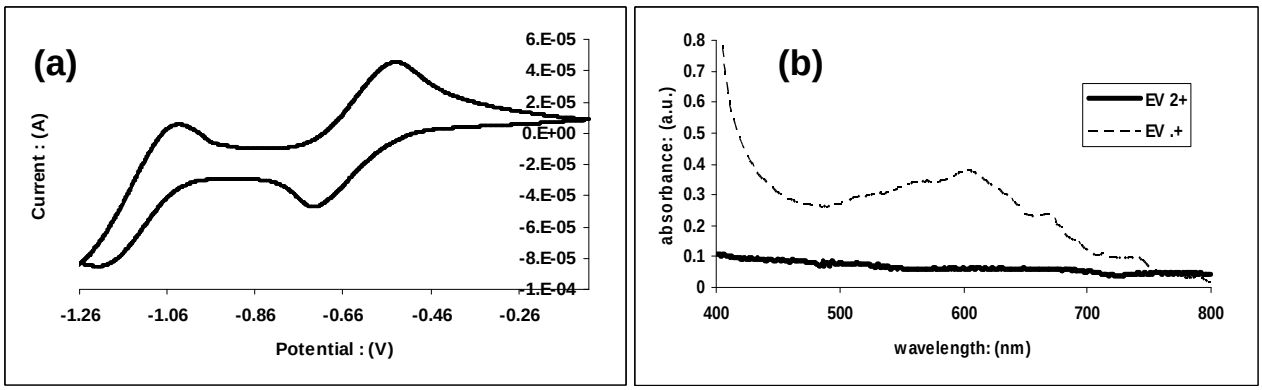

Fig. 5: (a) Cyclic Voltammogram obtained of EV dibromide in [emIm][fap]/SZ4 gel (b) Corresponding absorbance spectra of EV dibromide in [emIm][fap]/SZ4 gel.

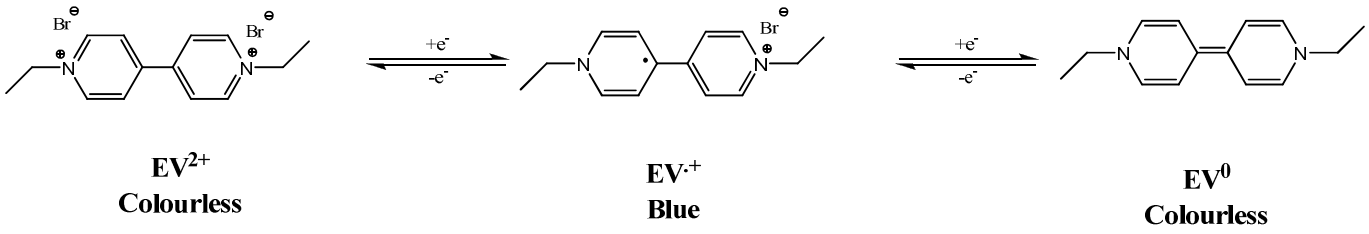

EV^{2+}
Colourless

$EV^{\cdot+}$
Blue

EV^{0}
Colourless

Scheme 2: The three distinct redox states of the ethyl viologen dibromide dye.

Spectroelectrochemistry was then performed on the electrochromic ionogel; which was directly dropcast and photopolymerised onto an ITO working electrode.

The resulting cyclic voltammogram (fig 5 (a)) displays the classical two reduction steps expected for viologen based devices[29, 30]. Equally, the UV/Vis spectra also show the clear difference between both the EV^{2+} and $EV^{\cdot+}$ redox states (fig 5 (b)). The radical cationic state was generated by maintaining the voltage current on the working electrode at the first reduction potential (in this case -0.7V). This resulted in the generation of a dark blue colour, and a strong absorbance around 600nm.

The next logical step therefore was the construction of the electrochromic device, where the photopatternable ionogel was expected to act as a solid electrolyte for the reversible viologen redox process.

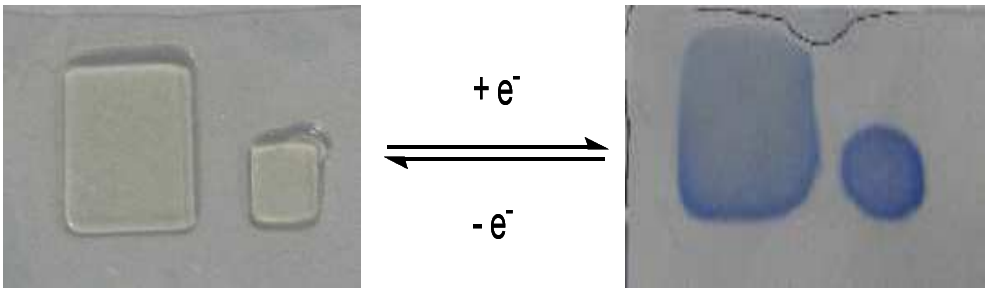

Fig. 6: Patterned electrochromic ionogels exhibiting reversible viologen redox states.

The fabrication process for the electrochromic device is described above. Once the device was complete it was connected to a power supply, the perturbation voltage was ~1V which resulted in the patterned squares turning blue (fig 6 (right)). The process was then reversed by changing the voltage bias or by simply turning off the current, resulting in the reformation of the colourless dicationic salt.

We have observed however, that the presumably unstable radical cation did not revert back to the colourless state immediately in the ionogel environment. The stabilisation of the viologen radical cation has been reported previously, and has been attributed to low concentrations of molecular oxygen in the supporting electrolyte and in its ability to form charge-transfer complexes with strong lewis bases[31]. Stabilisation of the dye has also been reported in IL based environments.

Shin et al claimed that an imidazolium based IL acts as an electron buffer that maintains low pH levels, thereby stabilising the reduced state[32].

Future work therefore; will be to monitor the kinetics of the reversion of the viologen dye to its dicationic form in different ionogel compositions, with a view to optimising these parameters for the development of future electrochromic devices.

Conclusion:

In summary, we have developed a facile method to photo-pattern ionogel materials containing phosphonium and imidazolium based ILs. Ionogels have been characterised by vibrational and electrochemical impedance spectroscopy, from these results the organic-inorganic matrix does not seem to affect the physical or chemical behaviour of the encapsulated IL. A particularly attractive quality of these ionogels is the ability to spatially define their precise location and structure by optical exposure. Tremendous potential lies in the ability to photopattern flexible opto-electronic materials with high precision. The incorporation of an electrochromic dye also highlights further future potential applications in the development of a patternable electrochromic display that functions with a comparatively low voltage perturbation signal.

Acknowledgement:

This work is supported by Science Foundation Ireland under grant 07/CE/I1147 including the SFI-funded National Access Programme (NAP) grant NAP210 and by Enterprise Ireland grant 07/RFP/MASF812, which is part of EU-MATERA initiative.

The Authors would like to thank Dr. Al Robertson of Cytec® industries for the generous donation of IL's used in this study, and Prof. Robert Forster and Dr. Colm Mallon for the generous use of instruments used to obtain key results

The authors would also like to thank Prof. Dr. Boris Chichkov and Dr. Alexandr Ovsianikov from the Lazer Zentrum Hannover for the access to the 2PP instrument, and Ciba® Chemicals for generously providing the photoinitiators employed in this study.

References:

1. S. T. Handy, *Curr. Org. Chem.*, 2005, **9**, 959-988.
2. H. Weingaertner, *Angewandte Chemie-International Edition*, 2008, **47**, 654-670.
3. C. Chiappe and D. Pieraccini, *Journal of Physical Organic Chemistry*, 2005, **18**, 275-297.
4. D. R. MacFarlane, M. Forsyth, E. I. Izgorodina, A. P. Abbott, G. Annat and K. Fraser, *Physical Chemistry Chemical Physics*, 2009, **11**, 4962-4967.
5. J. G. Huddleston, A. E. Visser, W. M. Reichert, H. D. Willauer, G. A. Broker and R. D. Rogers, *Green Chem.*, 2001, **3**, 156-164.
6. M. Armand, F. Endres, D. R. MacFarlane, H. Ohno and B. Scrosati, *Nature Materials*, 2009, **8**, 621-629.
7. M. Galinski, A. Lewandowski and I. Stepniak, *Electrochimica Acta*, 2006, **51**, 5567-5580.
8. J. C. Ribot, C. Guerrero-Sanchez, R. Hoogenboom and U. S. Schubert, *Journal of Materials Chemistry*, 2010, **20**, 8279-8284.
9. A. Vioux, L. Viau, S. Volland and J. Le Bideau, *Comptes Rendus Chimie*, **13**, 242-255.
10. C. Schmidt, T. Gluck and G. Schmidt-Naake, *Chemical Engineering & Technology*, 2008, **31**, 13-22.
11. M. Antonietti, D. B. Kuang, B. Smarsly and Z. Yong, *Angewandte Chemie-International Edition*, 2004, **43**, 4988-4992.
12. T. Ueki and M. Watanabe, *Macromolecules*, 2008, **41**, 3739–3749.
13. M. A. Neouze, J. Le Bideau, P. Gaveau, S. Bellayer and A. Vioux, *Chemistry of Materials*, 2006, **18**, 3931-3936.
14. F. Gayet, L. Viau, F. Leroux, S. Monge, J. J. Robin and A. Vioux, *Journal of Materials Chemistry*, 2010, **20**, 9456-9462.
15. S. V. Eliseeva and J. C. G. Bunzli, *Chemical Society Reviews*, 2010, **39**, 189-227.
16. M. J. Earle, J. Esperanca, M. A. Gilea, J. N. C. Lopes, L. P. N. Rebelo, J. W. Magee, K. R. Seddon and J. A. Widegren, *Nature*, 2006, **439**, 831-834.
17. R. Copperwhite, M. Oubaha, D. L. Versace, C. Croutxe-Barghorn and B. D. MacCraith, *Journal of Non-Crystalline Solids*, 2008, **354**, 3617-3622.

18. J. Serbin, A. Ovsianikov and B. Chichkov, *Optics Express*, 2004, **12**, 5221-5228.

19. A. Morrin, A. J. Killard and M. R. Smyth, *Analytical Letters*, 2003, **36**, 2021-2039.

20. G. Ehrhart, B. Capoen, O. Robbe, P. Boy, S. Turrell and M. Bouazaoui, *Thin Solid Films*, 2006, **496**, 227-233.

21. R. Byrne, C. Ventura, F. Benito-López, A. Walther, A. Heise and D. Diamond, *Biosensors and Biolelectronics*, 2010, **Submitted**.

22. P. E. Stallworth, J. J. Fontanella, M. C. Wintersgill, C. D. Scheidler, J. J. Immel, S. G. Greenbaum and A. S. Gozdz, *Journal of Power Sources*, 1999, **81**, 739-747.

23. L. A. Neves, J. Benavente, I. M. Coelhoso and J. G. Crespo, *Journal of Membrane Science*, 2010, **347**, 42-52.

24. M. Oubaha, R. Copperwhite, B. Murphy, B. Kolodziejczyk, H. Barry, K. O'Dwyer and B. D. MacCraith, *Thin Solid Films*, 2006, **510**, 334-338.

25. M. Oubaha, R. K. Kribich, R. Copperwhite, P. Etienne, K. O'Dwyer, B. D. MacCraith and Y. Moreau, *Optics Communications*, 2005, **253**, 346-351.

26. A. Vioux, L. Viau, S. Volland and J. Le Bideau, *Comptes Rendus Chimie*, 2010, **13**, 242-255.

27. C. L. Bird and A. T. Kuhn, *Chemical Society Reviews*, 1981, **10**, 49-82.

28. R. J. Mortimer and J. R. Reynolds, *Displays*, 2008, **29**, 424-431.

29. C. A. Melendres, P. C. Lee and D. Meisel, *Journal of the Electrochemical Society*, 1983, **130**, 1523-1527.

30. M. De Leo, L. M. Moretto, O. Buriez and P. Ugo, *Electroanalysis*, 2009, **21**, 392-398.

31. P. M. S. Monk and N. M. Hodgkinson, *Electrochimica Acta*, 1998, **43**, 245-255.

32. S. R. Shin, C. K. Lee, S. I. Kim, I. So, G. M. Spinks, G. G. Wallace and S. J. Kim, *Langmuir*, 2008, **24**, 3562-3565.